Sound dissimilar linear friction welding of A7075-T6 Al and mild steel by simultaneous interfacial deformation using higher forging speed

Furkan Khan, Takuya Miura, Tetsuro Ito, Yoshiaki Morisada, Kohsaku Ushioda, *Hidetoshi Fujii

Joining and Welding Research Institute, Osaka University, Osaka, Japan, 567-0047.

*Corresponding author's email address: fujii.hidetoshi.jwri@osaka-u.ac.jp

Abstract

Sound dissimilar welding of heat-treatable A7075-T6 aluminum and mild steel is extremely difficult due to the formation of interfacial cracks. The present study aims to attempt linear friction welding (LFW) of high-strength A7075-T6 Al alloy and mild steel to obtain sound joints with the highest strength ever by controlling the quality deteriorating phenomena that previous studies have faced. In this study, LFW joints were fabricated under two different applied pressures of 100 MPa and 300 MPa at forging speed of 5 mm/s, along with various forging speeds ranging from 5 mm/s, 10 mm/s, to 20 mm/s under pressure of 300 MPa, and the joint microstructure, mechanical properties and interface macrostructure were investigated. Furthermore, thermal dependence behaviors of both alloys were systematically investigated to optimize the processing parameters, especially applied pressure during LFW. At lower forging speeds of 5 mm/s and 10 mm/s, the weld defects and un-bonded regions were observed near the center of the weld accompanying to unevenness of butt surface due to the relatively thick intermetallic compound (IMC) formed in the interface which greatly influenced the joint strength. In contrast, at higher forging speed of 20 mm/s, weld defects at the joint interface were effectively suppressed by promoting the simultaneous and uniform interfacial deformation of both alloys thanks for the extremely thin IMC during LFW. Consequently, a highly efficient joint with 100 % efficiency was successfully obtained at higher forging speed of 20 mm/s and despite the occurrence of softening towards A7075, the fabricated

joint displayed a base metal fracture towards the steel side.

Keywords: Linear friction welding, dissimilar welding, 7075-T6 Al alloy, steel, microstructure, mechanical properties

1. Introduction

Considerable efforts have recently been made worldwide to reduce the amount of CO_2 emissions to the atmosphere. One of the most effective ways to suppress CO_2 emission is the weight reduction of vehicles, and joining dissimilar materials has been accepted as one of the most representative methods for weight reduction. Therefore, the demand for dissimilar joints of steel and aluminum is rapidly increasing especially for transportation industries such as automotive, aerospace, aviation, railway, and shipbuilding for weight reduction, improved fuel efficiency, environmental concern, energy saving and cost saving [1–6]. Steels and aluminum alloys represent the highly preferred dissimilar couple of alloys within the automotive sector [7,8]. Among various Al-alloys, heat-treatable A7xxx series aluminum alloys are of significant interest in transportation industries due to their natural ageing characteristics and high strength-to-weight ratio [9]. Furthermore, A7075 is renowned for its remarkable toughness and excellent fatigue resistance [10]. Therefore, fabricating a sound dissimilar joint between A7075 and steel would offer significant advantages in producing robust and cost-effective structural components. Welding these alloys, however, is associated with a range of weld defects, including hot cracking and porosity. Among these, hot cracking is the most critical issue that can substantially influence joint strength and, consequently, overall structural safety [11]. This would make conventional fusion welding, which is accompanied with high heat input and comprises melting of parent material, an inefficient

technique to join these alloys. The principal issues of conventional fusion welding methods for joining steel to aluminum are the occurrence of solidification cracking, porosity, and formation of brittle intermetallic compound (IMC) layer, which with increasing thickness, increases crack susceptibility and remarkably deteriorates the performance of the produced joints. Therefore, the mechanical properties of steel and aluminum weld are sensitive to IMC layer thickness and faying surface defects. Yang et al. [12] investigated the control of interfacial layer uniformity to weld A6061-T6 with 301 stainless steel using hybrid laser-metal inert gas technique. It was reported that interfacial layer with a most uniform thickness of $\sim$5.2 μm could be obtained and the joint exhibited relatively low tensile strength of ~70% of the Al base metal. On the other hand, efforts were made to join steel with Al alloys using resistance spot welding (RSW) [13], and magnetic-assisted resistance spot welding (MA-RSW) [14]. It was revealed that welds made with an external magnetic field exhibited enhanced strength compared to welds made with no external magnetic field. However, significantly thick IMC layers of ~9.14 μm and ~6.59 μm were observed at steel-aluminum joining interface in RSW and MA-RSW, respectively, containing pore defects at both RSW and MA-RSW nuggets along the IMC/Al weld nugget interface.

On the other hand, multiple attempts such the utilization of frictional welding methods, such as friction stir welding and rotary friction welding method, and the incorporation of joining interlayers have been made to achieve base metal fracture. Numerous investigations on those friction welding methods of steel with aluminum alloys, primarily through intermetallic compound (IMC) formation, have shown that the thickness of the IMC layer significantly influences the strength of such dissimilar joints. Herbst et al. [15] carried out investigation on friction welds between 20MnCr5 steel and

AW6082 aluminum alloy by changing the IMC layer thickness through solution annealing and aging and reported a reduction in joint strength with the increase of mean IMC thickness. Also, Tanaka et al. [16] conducted several experiments on dissimilar A7075-T6 and mild steel FSWed joints to investigate and analyze the relationship between joint strength and IMC layer thickness. It was reported that the joint strength increased exponentially with the reduction of IMC layer thickness. Additionally, despite the formation of an extremely thin IMC layer, it was nearly impossible to obtain a joint that exhibited a base metal fracture [16]. On the other hand, multiple attempts such a utilization of alternative friction welding methods, such as rotary friction welding method, and the incorporation of joining interlayers have been made to achieve base metal fracture. Kawai et al. [17] performed friction welding of low carbon steel (S25C) with different series of Al alloys (i.e., 2xxx, 5xxx, 6xxx, and 7xxx) using rotary friction welding method and reported that dissimilar joints of A7075-T6 with S25C revealed poor friction weldability with a maximum joint efficiency ranging from 20 - 40 %. Thick brittle IMCs of Al-Cu-Fe were found to be formed at the weld interface, causing poor friction weldability. Kimura et al. [18] introduced an interlayer of pure aluminum of A1070 type between the base materials to fabricate joints without the formation of IMC layer at the interface; however, joint strength was far below that of the steel base metal strength. Additionally, interfacial deformation predominantly occurred on the A7075 side only, while low-carbon steel (LCS) side exhibited minimal or negligible interfacial deformation. In friction welding technology, in addition to the thickness of the IMC layer at the weld interface, the plastic deformation behavior of each material around the joint greatly influences the joint strength. Kimura et al. [19] examined the possibility of obtaining a sound dissimilar joint between A7075-T6 and low carbon steel (LCS) using rotary friction

welding method and investigated the effect of friction welding conditions on the tensile strength of fabricated joints. Although using identical parameters for joint fabrication, the joint strength exhibited scattering and obtaining a sound joint was extremely difficult, primarily because the generation of cracks in the A7075-T6 flash attributed to the poor plastic deformation ability of A7075. These findings suggested that in order to obtain a strong dissimilar joint between A7075-T6 and steel successfully, it is effective not only to reduce the thickness of IMC layer but also to suppress crack formation by generating uniform deformation around the critical weld interface.

Linear friction welding (LFW) is a frictional solid-state joining method in which a joint is fabricated through the relative motion of two components under a high contact load. It means, there is no melting of the parent material. So common problems associated with fusion welding such as solidification cracking and porosity are avoided. The first patent of LFW process was applied in 1929 [20]. Although this patent was associated with a vague description, the patent tailored for LFW equipment was officially licensed in 1969 [21]. Following the manufacturing of specialized LFW equipment at The Welding Institute (TWI) in the early 1980s, the development of the LFW technique advanced primarily with a focus on its application in aerospace, particularly with titanium and nickel alloys [22–24]. The LFW process possesses numerous appealing features such as no welding tool is required for the welding of materials, this characteristic is very useful for the welding of high-melting point materials such as steel, while the wide applicability of friction stir welding (FSW) is still limited by the tool durability for these materials. Extremely short welding time of less than 1 s, as the weld can be achieved within a fraction of second, it could be very beneficial to manufacturing industries for mass production and cost saving. The ability to achieve high reproducibility with high

dimensional accuracy of the joint. Furthermore, while the wide applicability of conventional rotary friction welding is still limited to round-shaped specimens, it is adaptable for use with non-axially symmetrical objects as well. Besides, LFW is a self-cleaning welding process. All the process impurities or oxides which could be present at the weld interface are expelled with the generated flash outside the weld interface. Thus, the preparation of the welding joint is minimal and LFW can be done in open air, no gas shield is required. LFW stands out as a highly automatable and consistently repeatable process. This is attributed to its sole reliance on a mechanical heat source, ensuring that all energy input is meticulously controlled through motion and loads. Certainly, through the welding of near-net-shape parts, LFW enables significant mass savings, a decrease in machining costs, and consequently, substantial overall cost savings.

Using LFW method, the interfacial deformation characteristic of welding alloys can be uniquely controlled by controlling the applied pressure during welding [25]. This characteristic is expected to be also very effective to obtain sound dissimilar welding, such as between various titanium alloys [26,27], steel and aluminum alloys. LFW involves expelling the interfacial material in the form of flash. Typically, when dissimilar materials are joined by LFW or other friction welding methods, only the material with lower strength preferentially deforms at the joining temperature and is ejected as flash whereas, no interfacial deformation occurs on the faying surface of high-strength material [28,29]. As a result, oxides and rugged surfaces may remain at the bonding interface due to the absence of simultaneous and uniform interfacial deformation of materials during welding which can adversely affect the joint properties. On the other hand, simultaneous deformation of both base metals, by adjusting the applied pressure corresponding to temperature where the base metal strengths are equal, can be obtained and sound joint

between dissimilar materials can be achieved during LFW as reported by Fujii [25]. Additionally, Lim et al. [30] controlled the deformation behavior of AA5052 and S45C steel using pressure-controlled joule heat forge welding (PCJW), which is a solid-phase welding method by heat generation and upset near the butt interface as in LFW, and reported that simultaneous and uniform interfacial deformation of both materials during welding is of utmost importance in order to enhance joint strength of dissimilar welds. Therefore, in the present study, as further investigation, the primary emphasis was placed on promoting the simultaneous interfacial deformation of both steel and A7075 during LFW to obtain sound joint. Hence, to achieve simultaneous interfacial deformation of both alloys, forging speed was varied keeping the applied pressure constant at 300 MPa during LFW.

The present study aims to attempt linear friction welding of high-strength A7075-T6 Al and mild steel in order to produce a sound dissimilar joint. In addition to optimizing the applied pressure based on the temperature dependence in strength of mild steel and A7075 Al alloy, the effect of forging speed on joint strength and uniform deformation and weld defects formation at the joint interface have been clarified. Unlike to conventional LFW, where frictional heating of the material and flash ejection are distinguished by increasing the applied pressure between the burn-off phase and the forging phase. In this study, the control of welding thermal history based on the balance between temperature-dependent material strength and flash ejection rate is realized by using constant applied pressure. Moreover, the influence of variable forging speed on steel and aluminum weld was investigated which was never reported before during LFW.

2. Experimental procedure

2.1 Test materials

Precipitation strengthened high strength JIS A7075-T6 Al alloy (hereinafter referred to as A7075) and JIS SPHC mild steel (hereinafter referred to as steel) specimens with dimensions of 67 mm^{L} x 20 mm^{W} x 5 mm^{T} were used as base metals (BMs) to produce a linear friction welding (LFW) joint. Table 1 shows the chemical compositions (wt. %) and ultimate tensile strength (UTS) of the base metals. The 5 mm x 20 mm face was used as the friction surface, and A7075 was provided reciprocation motion during LFW. The faying surfaces of both materials were cleaned using acetone and ethanol.

Table 1. Chemical compositions (wt. %) and UTS of the base metals selected in this study.

Material	**Si**	**Fe**	**Cu**	**Mn**	**Mg**	**Cr**	**Zn**	**Ti**	**Al**	**UTS (MPa)**
A7075-T6	0.08	0.19	1.5	0.04	2.2	0.19	5.8	0.03	bal.	589
Material	**C**	**Si**	**Mn**	**P**	**S**	**Fe**				**UTS (MPa)**
Mild steel	0.05	0.005	0.24	0.015	0.007	bal.				347

Thermal dependences of ultimate tensile strength (UTS) of the mild steel and A7075 were evaluated by a high-temperature tensile test. High-temperature tensile tests were conducted from room temperature to 350℃ and 600℃ for A7075 and steel, respectively, using tensile testing machine (AGS-X 10 kN, SHIMADZU) with comparatively small size tensile specimens of 5 mm gauge length, 2 mm gauge thickness and 2 mm gauge width.

2.2 Process parameters

The specimens were linear friction welded using LFW equipment (Model Number; 8AT2020A00, TOYO KOGYO) under the different applied pressures of 100 MPa and 300 MPa, determined based on the results of the evaluation of the temperature

dependence of the UTS of the base metals shown in later chapters, at the constant forging speed of 5 mm/s (the forging speed is the pressing speed of materials along the length during LFW process), with constant upset and oscillation frequency of 5 mm and 50 Hz, respectively. The LFW was further conducted keeping the applied pressure constant at 300 MPa with different forging speeds of 5 mm/s, 10 mm/s, and 20 mm/s. Additionally, upset and oscillation frequencies were kept constant at 5 mm and 50 Hz, respectively. It is worth mentioning that for each welding condition, three replicates were produced in order to confirm the repeatability and consistency of the LFW joint. LFW method typically comprises four phases, as illustrated in schematic Fig. 1. Initially, both materials brought in contact with each other. In the conditioning phase, oscillation motion starts, generating frictional heat due to the relative motion of two components under high contact force. The generated frictional heat and force at the interface of two components causes materials to plasticize and deform at the interface. Due to the synergistic effect of applied load and specimen movement, most of the plasticized material is expelled away as flash from the weld interface region during the burn-off phase and forge phase. Therefore, the removal of surface oxides and other impurities from weld interface along with plasticize materials permits metal-to-metal contact with fresh surfaces of specimens and allows a joint to form. In conventional LFW, frictional heating of the material and flash ejection are distinguished by increasing the applied pressure between the burn-off phase and the forging phase [31]; however, in this study, the control of welding thermal history based on the balance between temperature-dependent material strength and flash ejection rate is realized by using constant applied pressure.

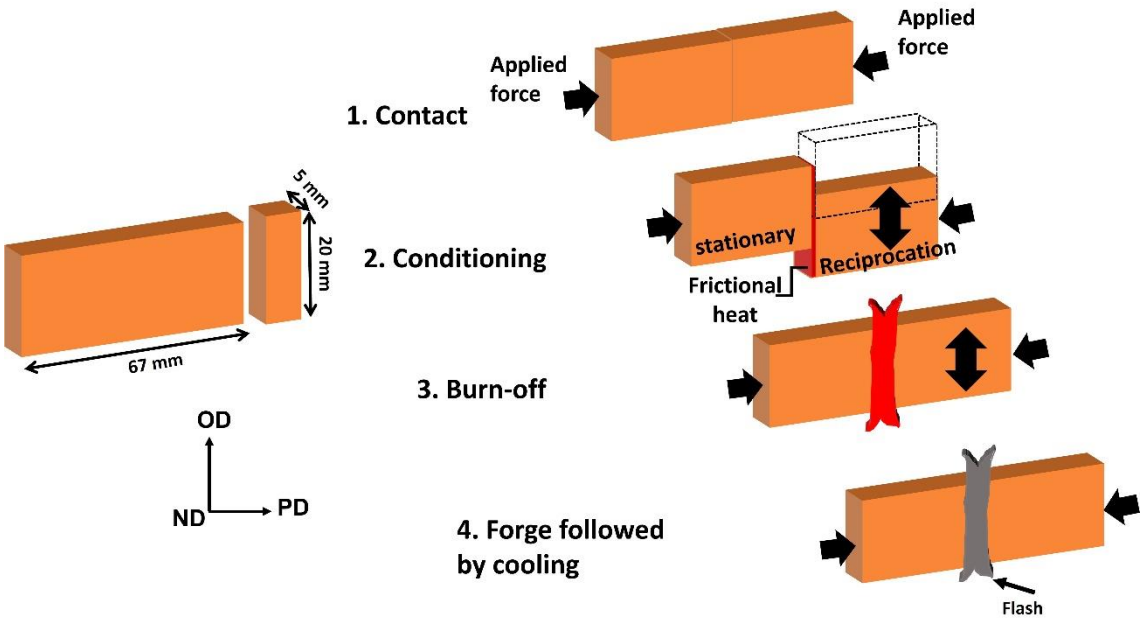

Fig. 1 Schematic illustration of four different stages of LFW process and dimensions of the used specimens.

2.3 Microstructure and mechanical characterization

To evaluate the joint strength of the produced welds, tensile test specimens were prepared across the joint interface using electric discharge machine (EDM; Sodick AG360L) with a gauge section of 2 mm thick, 3 mm wide and 20 mm long. Tensile testing was conducted at room temperature with a cross-head speed of 1 mm/min using a tensile test machine (AGS-X 10 kN, SHIMADZU). Furthermore, from the obtained joints, longitudinal cross-sectional specimens containing complete weld interfaces were cut using EDM machine and mechanically polished with abrasive papers up to 4000 grit, followed by 1 μm diamond suspension. A field emission scanning electron microscope (FE-SEM; JSM-7001FA, JEOL) was employed to observe the morphology of the joints interface. Additionally, thin foil specimens, with a thickness of 0.1 μm, were sectioned from selected regions of the joints interface using a focused ion beam machine (FIB; JIB-4500, JEOL) in order to characterize the intermetallic compounds (IMCs) formed using

a transmission electron microscopy (TEM; JEM-2100F, JEOL). Moreover, the obtained cross-section specimens were subjected to Vickers hardness testing at a load of 0.98 N with a dwell time of 15 s using a hardness tester (FM-800, FUTURE-TECH).

3. Results and discussion

3.1 Temperature dependence of base metals and relation between applied pressure

Fig. 2 shows the temperature dependence behavior of UTS of mild steel and A7075 evaluated by high-temperature tensile test. A7075 is composed of Al-Zn-Mg-Cu system, and its strength is mainly controlled by the presence of strengthening precipitates [32]. In addition, the melting point is about 660°C (933K), and the material softens rapidly at about 200°C. In contrast, mild steel is not strengthened by precipitates, so there is almost no reduction in strength at temperatures below 400°C. As a result, the UTS of mild steel and A7075 are reversed at room temperature and high temperature, and the curves expressing the temperature dependence of UTS have an intersection point around 220°C-300 MPa. In the case of 100 MPa applied pressure, according to the temperature dependence, A7075 started to deform when the interface temperature exceeded ~320℃ because the strength of A7075 dropped below the applied pressure (100 MPa). On the other hand, corresponding to ~320℃ strength of steel is maintained quite high as compared to A7075. Therefore, to facilitate deformation towards steel side at this temperature (~320℃), the minimum required applied pressure is ~290 MPa which is moderately higher than 100 MPa. As a result, only A7075 is ejected as flash without interfacial deformation on steel side during burn-off and forge phases. In the case of 300 MPa applied pressure, mild steel and A7075 are expected to deform simultaneously when the temperature reached to ~220°C. Therefore, the applied pressure of 300 MPa was

selected as the optimum one in this study, and the applied pressure of 100 MPa was for comparison.

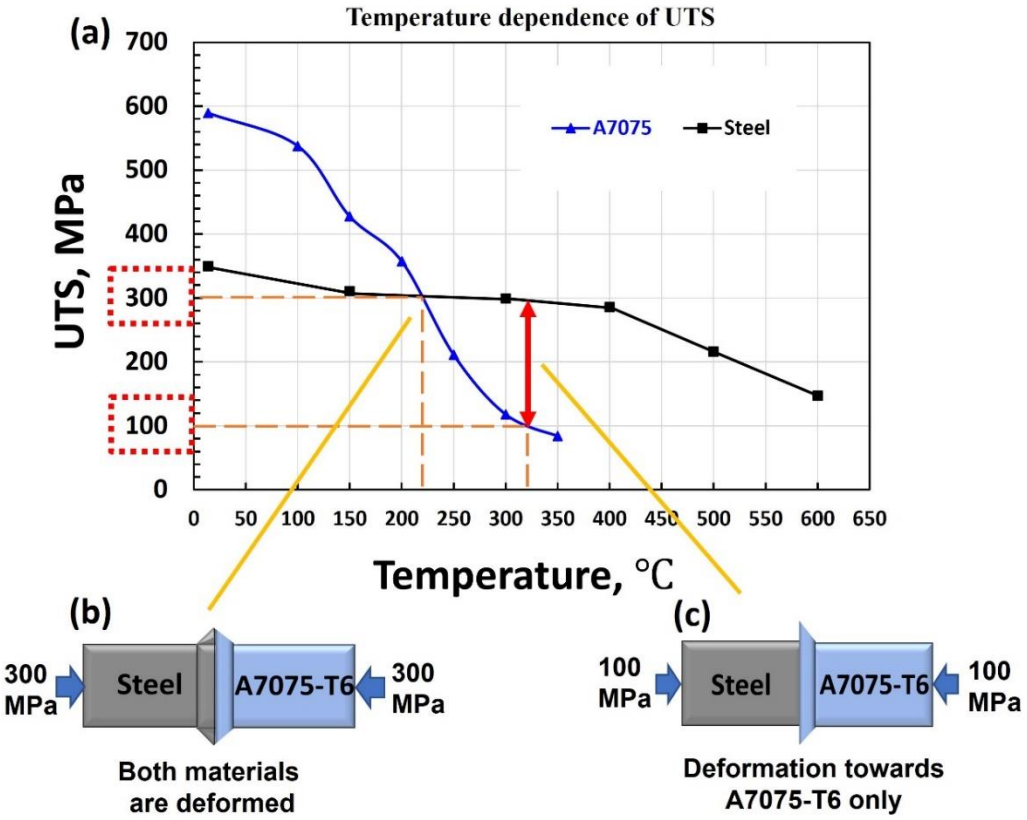

Fig. 2 (a) Thermal dependence behavior of ultimate tensile strength of mild steel and A7075, and the schematic illustrations of relationship between applied pressure and materials deformation during LFW at (b) 300 MPa, (c) 100 MPa applied pressure.

3.2 Forging speed and its relation between welding time

Fig. 3 shows the graphs of applied forging speed, upset stroke, and required welding time during the LFW of the joints fabricated at different forging speeds of 5 mm/s, 10 mm/s, and 20 mm/s with constant objective applied pressure of 300 MPa. Upset and oscillation frequency were kept constant at 5 mm and 50 Hz, respectively. The welding was completed as soon as the designated upset of 5 mm was achieved as shown in Fig.

3b, after achieving the targeted upset the forging speed rapidly fell to zero, Fig. 3a. The required welding time rapidly decreased as the forging speed increased, Fig. 3c. It is observed that the required welding time is lowest at a forging speed of 20 mm/s. Additionally, the weld completion time of 20 mm/s joint is just 0.4 s, whereas the time taken for the joints fabricated at 10 mm/s and 5 mm/s forging speed was observed to be 0.76 s and 1.18 s, respectively. Recently, significant conclusions have been provided to obtain sound welding of A7075 alloys by utilizing the highest possible welding speed in order to reduce the welding time [33], as the faster the welding speed, the less time the weld is in hot cracking range [33,34].

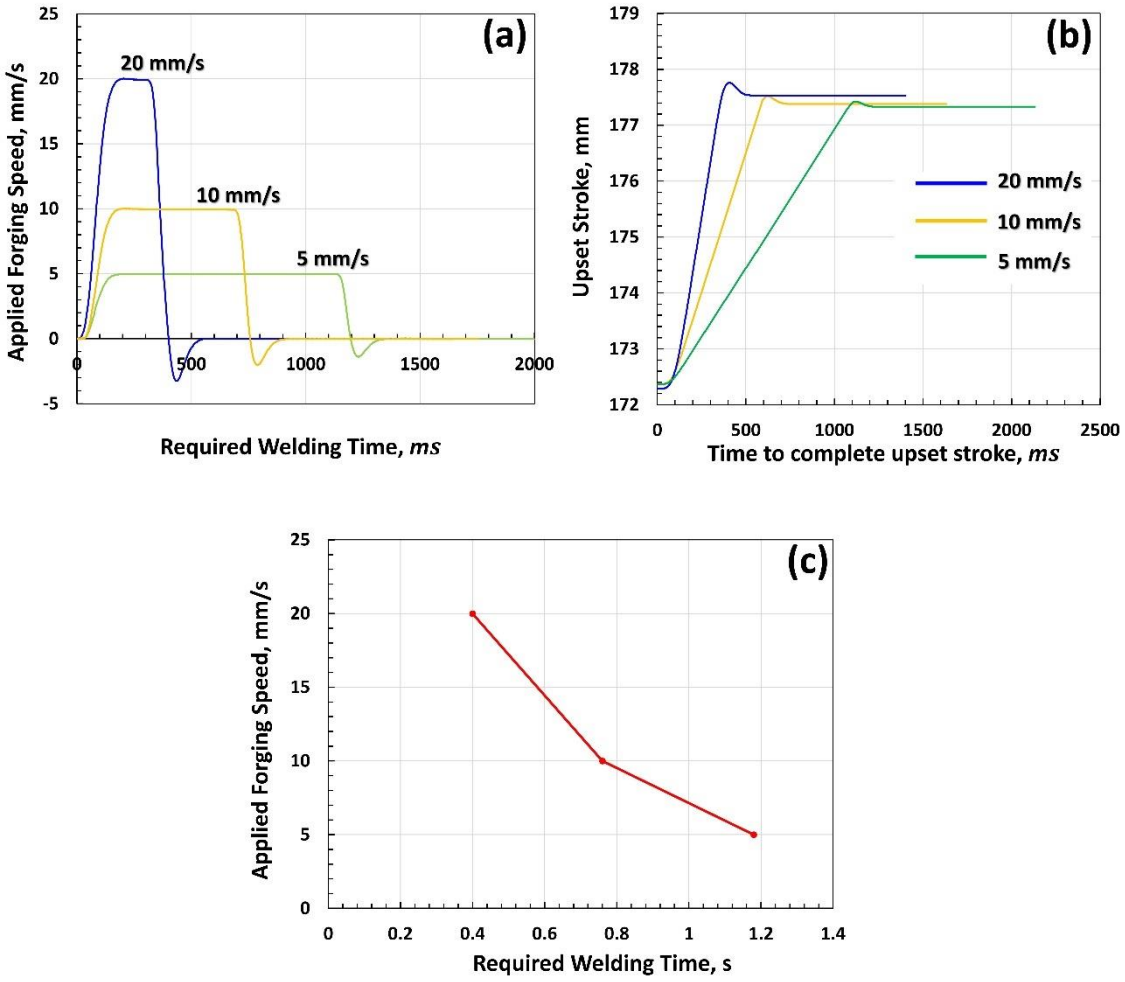

Fig. 3 (a) Relationship between applied forging speed and required welding time, (b) relationship between upset stroke and time required to complete the upset stroke at different forging speeds of 5 mm/s, 10mm/s, and 20 mm/s, (c) corresponding required welding time at respective forging speed.

Moreover, it is noteworthy that shortly after the completion of the A7075/steel joining, a noticeable discontinuous cracking sound can be heard, particularly under certain specific joining conditions. This cracking sound is attributed to the thermal contraction experienced during the solid-state cooling of A7075. A7XXX has been recognized as one of the aluminum alloy series most susceptible to thermal residual stresses [35]. While this cracking sound can be noticeably heard in the weld fabricated at 5 mm/s and 10 mm/s forging speed. In contrast, it was effectively suppressed in joint

fabricated at higher forging speed of 20 mm/s.

3.3 Joint appearance

Fig. 4(a-d) shows the joint appearance of the welds obtained at different applied pressure of 100 MPa with 5 mm/s forging speed, and 300 MPa with forging speeds ranging from 5 mm/s, 10 mm/s, and 20 mm/s at constant upset and constant oscillation frequency of 5 mm and 50 Hz, respectively. A7075 consistently displayed significant interfacial deformation during weld fabrication process. The extent of deformation towards steel side is shown by the blue dotted lines in Fig. 4(a-d). It is noteworthy that the weld fabricated at an applied pressure of 100 MPa exhibited almost no interfacial deformation towards the faying surface of steel. In contrast, A7075 experienced severe interfacial deformation during welding as shown in Fig. 4a. This finding was attributed to the fact of the notable difference in strength between mild steel and A7075 as shown in Fig. 2, similar observations were reported by Matsuda et al. [36] during LFW of 304 stainless steel with A6063 and A5083 Al alloys. Because steel showed no interfacial deformation during welding, it is possible that oxides and rugged surfaces may have persisted at the joining interface. On the other hand, at 300 MPa applied pressure, the deformation mode near the faying surface of mild steel was changed with the increased forging speed. At a forging speed of 5 mm/s and 10 mm/s, steel exhibited gradient deformation in which the deflection gradually decreases with increasing distance from the joint interface as shown in Fig. 4b and 4c. In contrast, A7075 again exhibits severe interfacial deformation almost same with 100 MPa case. It is noteworthy that at 20 mm/s forging speed, steel experienced severe deformation that resulted in a uniform ejection of flash perpendicular to the upset direction of specific range of material in the vicinity of

the butt interface simultaneously with A7075 without gradual deflection, Fig. 4d.

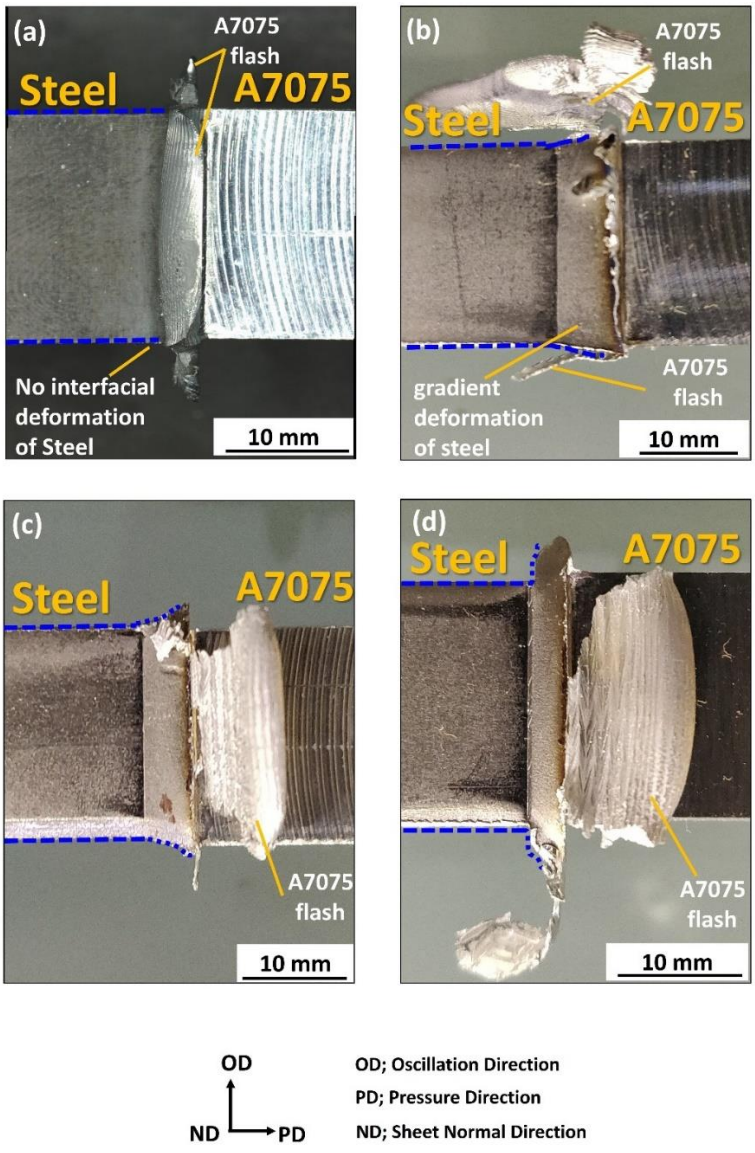

Fig. 4 Appearance of longitudinal cross sections of the joints fabricated at an applied pressure of (a)100 MPa and 5 mm/s forging speed, (b) 300 MPa and 5 mm/s forging speed, (c) 300 MPa and 10 mm/s forging speed, (d) 300 MPa and 20 mm/s forging speed.

3.4 Joint tensile strength

Tensile tests were conducted to evaluate the tensile strength of the obtained joints. The testing direction was perpendicular to the direction of weld line and the tests were

performed at a cross-head speed of 1 mm/min. The tensile specimens were taken as shown in the schematic Fig. 5c after removing flash.

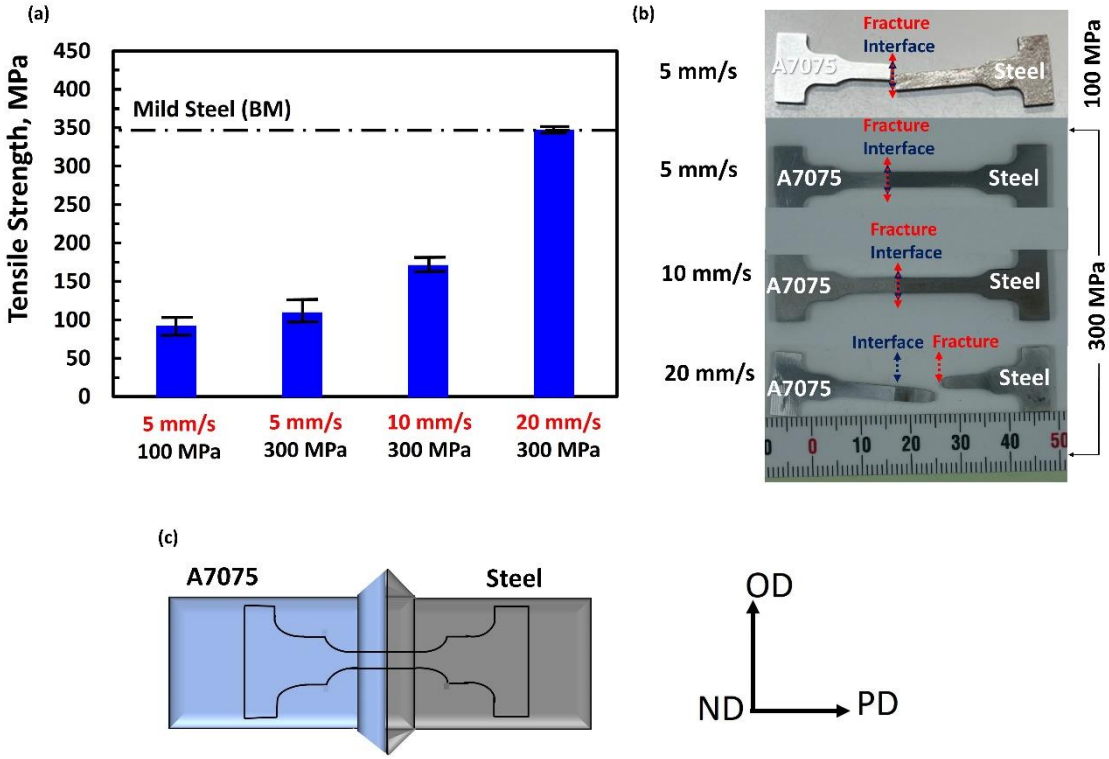

Fig. 5 (a) Tensile strength of the obtained joints, (b) fractured tensile specimen of the weld fabricated at different forging speeds and applied pressure, (c) schematic and location of tensile test specimen.

The joint obtained at 100 MPa exhibited a joint strength of ~92 MPa. The much lower strength at an applied pressure of 100 MPa can be attributed to the absence of interfacial deformation towards faying surface of steel during welding which leads to partial joining of weld interface. Whereas the joint fabricated at an applied pressure of 300 MPa with forging speeds of 5 mm/s and 10 mm/s showed a bit improvement in the joint strength and exhibited a tensile strength of ~109.2 MPa and 170.7 MPa as shown in Fig. 5a. However, the weld strength is still far below than that of the steel BM (347 MPa). Fig. 5b shows the fractured tensile specimens. The fracture location and weld

interfaces are denoted by dotted double-sided red and blue arrows, respectively. The joints fabricated at lower forging speeds of 5 mm/s and 10 mm/s exhibited an interfacial fracture. In contrast, the weld produced at a forging speed of 20 mm/s revealed an average tensile strength of ~347.1 MPa with base metal fracture towards the steel side. Additionally, tensile tests were performed to confirm the joint strength near the peripherical location of the weld produced at a forging speed of 20 mm/s using relatively smaller tensile specimens with gauge length, width, and thickness of 6 mm, 2 mm, and 2 mm, respectively. The weld revealed an average joint strength of ~347 MPa and the fracture was located in the base metal region of steel, which is comparable and consistent with the joint strength at the weld center.

Fig. 6 shows the joint efficiency of precipitation-strengthened A7075 and steel weld achieved so far employing direct rotary friction welding method and using pure Al as an interlayer material [17–19,37,38]. The current research is indicated by the red-dotted lines in Fig. 6. The weld joints obtained previously suffer from poor joint efficiency and several joint defects such as interface cracking that reached to the weld interface [19]. In the current study, the tensile strength of the joint obtained by using LFW method was equal to the mild steel base metal, which exhibited 100 % joint efficiency with respect to steel. It is indeed surprising to achieve such a highly efficient dissimilar joint between steel and A7075. To the best of author's knowledge, this is the first time to achieve 100 % joint efficiency of steel and A7075 dissimilar joint employing LFW method and exhibiting a base metal fracture towards steel side.

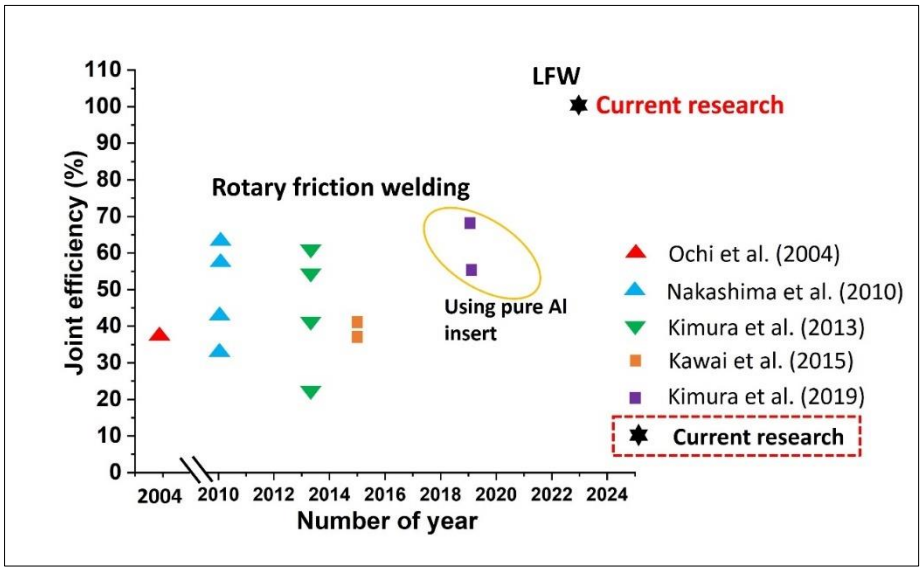

Fig. 6 Joint efficiency of dissimilar A7075/steel weld achieved so far using other pressure-controlled solid-state welding method (Rotary Friction Welding). Joint efficiency obtained in the current research is indicated by red-dotted rectangle.

3.5 Microhardness distribution

Fig. 7 shows the Vickers hardness distribution, as a function of distance from the weld center line, of the joints obtained at constant applied pressure of 300 MPa with different forging speeds of 5 mm/s, 10 mm/s, and 20 mm/s. The lowest hardness values in each joint were consistently observed towards the steel side, which coincides with the fracture location of the 20 mm/s joint that exhibited the highest strength in the tensile test. Regardless of the forging speed employed, all joints exhibited a notable increase in microhardness near the joint interface towards steel side. The peak hardness value of ~211 Hv was observed at a forging speed of 20 mm/s near the joint interface towards steel side.

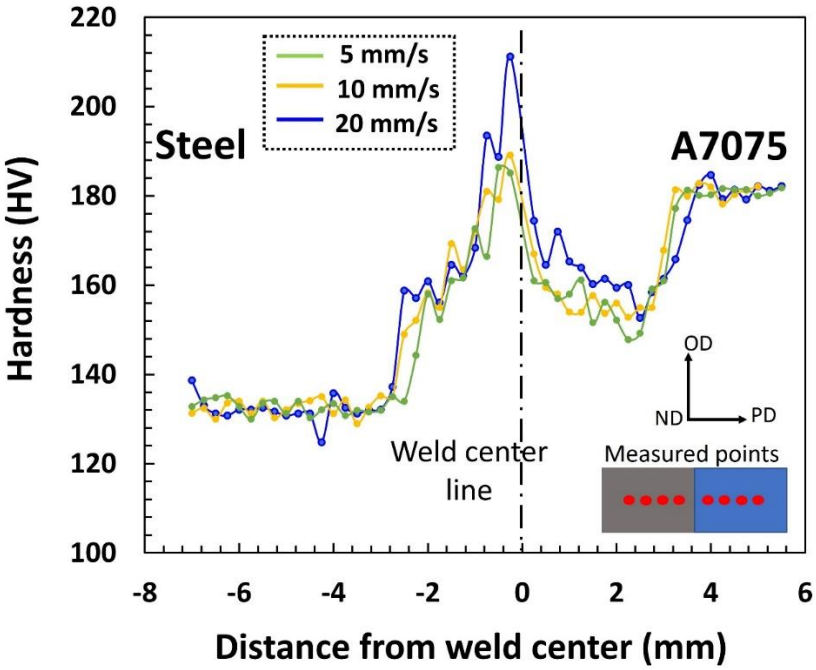

Fig. 7 Microhardness distribution across the interfaces of the joints fabricated at an applied pressure of 300 MPa and different forging speeds of 5 mm/s, 10 mm/s, and 20 mm/s.

On the other hand, the A7075 base metal (BM) was in T6 heat-treated condition. It is well known that by T6 heat treatment of A7075 aluminum alloys, artificially new precipitates form in the microstructure, thereby enhancing strength. However, softening occurred towards the A7075, which can be attributed to the dissolution of strengthening precipitates due to high welding temperature during LFW process. Notably, average hardness value in the softened region was slightly improved at higher forging speed of 20 mm/s compared to 5 mm/s and 10 mm/s. Therefore, it is potentially a positive sign to partially suppress the softened region at comparatively high forging speed when considering welding A7075 with other types of high-strength steel alloys. It is worth noting that despite the occurrence of softening towards A7075, in case of the joint fabricated at 300 MPa applied pressure with 20 mm/s forging speed, the fracture was located in the steel base metal because the lowest microhardness in softened region was

always maintained above the base metal hardness of steel. This can be attributed to the remained precipitates in softening zone and reprecipitation during cooling process.

3.6 Joint interface macrostructure analysis

Fig. 8(a-h) shows the SEM images of the cross-section of fabricated joint interfaces. The presence of any weld defects and un-bonded areas were identified. Fig. 8a shows the joint interface fabricated at lower forging speed of 5 mm/s with an applied pressure of 100 MPa. The un-bonded joint interface is indicated by red arrows in Fig. 8a. Several un-bonded spots were identified throughout the weld interface including towards the edge portion of the weld as shown in Fig. 8e. Furthermore, Fig. 8(b-d) depicts the interface of the joints fabricated at an applied pressure of 300 MPa with different forging speeds of 5 mm/s, 10 mm/s, and 20 mm/s, respectively. Despite slight deformation of the steel side in appearance as shown in Fig. 4b, the butt surfaces are greatly deformed and show uneven shapes, voids and un-bonded areas. These defects, as shown in the red dotted rectangle in Fig 8b, are presumably caused by the unevenness of the faying surfaces. Additionally, un-bonded areas were observed at the edge portion of the joint, indicated by a red dotted ellipse. In Fig. 8g, the interface line of steel/A7075 weld is indicated by the white arrows. Further, increasing the forging speed to 10 mm/s (Fig. 8c), the joint defects were significantly suppressed. The joint was obtained well bonded near the edge of the weld. However, the voids were observed near the center of the weld accompanying to unevenness of butt surface, as shown by the red solid rectangle in Fig. 8h. These un-bonded regions would have greatly reduced joint strength. Further increasing the forging speed to 20 mm/s resulted in complete suppression of voids and cracks leading to a sound dissimilar joint without any interfacial defects as shown in Fig. 8d.

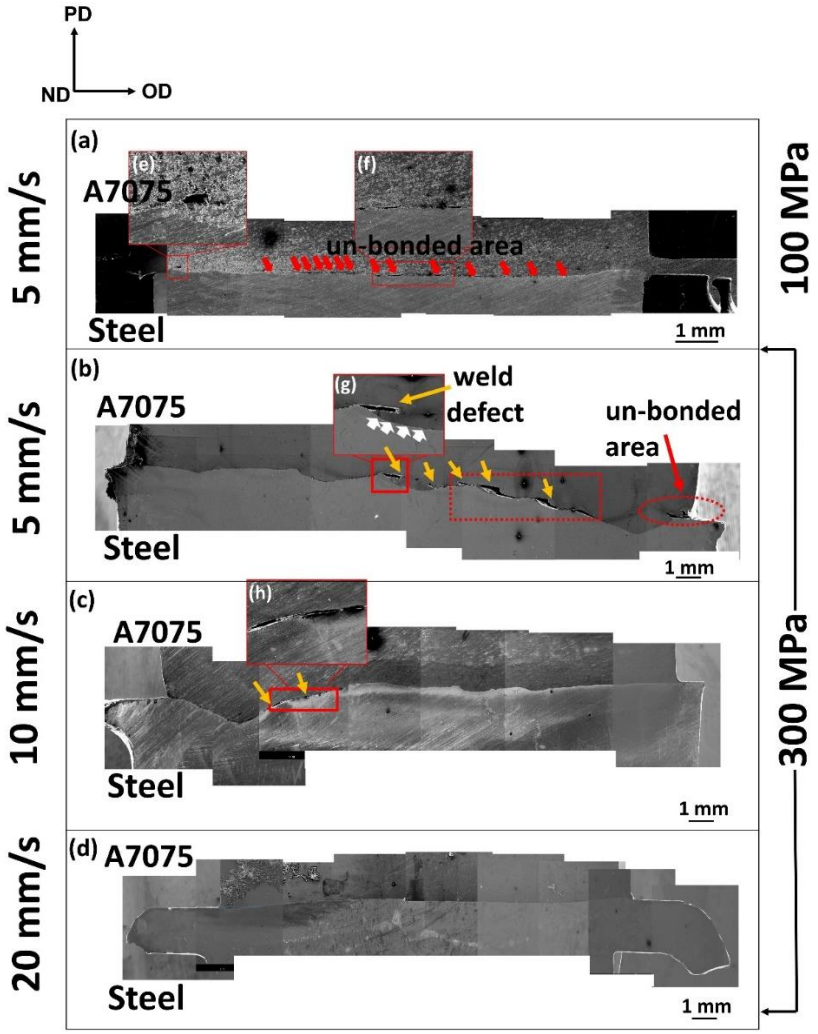

Fig. 8 SEM images of the weld interface of the joints fabricated at 100 MPa and 300 MPa applied pressure with different forging speeds of 5 mm/s, 10 mm/s, and 20 mm/s.

Additionally, it is noted that the weld interface fabricated at a comparatively high forging speed of 20 mm/s appears to be quite flat without any uneven segments. This difference in the flatness of the joint interface at low and high forging speeds can be correlated with the difference in the deformation mode on the steel side, as shown in Fig. 4, i.e., gradual deformation mode versus uniform flash ejection mode. In the uniform flash ejection mode, the steel and Al alloy deform in parallel directions as flash, which is thought to result in the formation of a flat interface. In the gradual deformation mode, the deformation on the

steel side is insufficient and uneven with the deformation on the Al side, leading to the formation of interface irregularities and un-bonded areas. The reasons why the forging speed affects the interface deformation mode will be discussed in section 3.7. The presence of un-bonded areas observed in low applied pressure or low forging speed conditions is considered to be the main reason for the significant decrease in tensile strength of the welding interface. Thus, it is clear that the formation of a flat joint interface with uniform flash ejection mode is effective for obtaining sound dissimilar steel/Al LFW joints.

3.7 TEM analysis of the interface and mechanism for improving bonding strength by increasing forging speed

The mechanism for improving the bonding strength by increasing forging speed is discussed in this section. Fig. 9 shows the TEM images and corresponding TEM-EDS line analysis of the interfaces of joints fabricated at an applied pressure of 300 MPa and different forging speeds of 5 mm/s, 10 mm/s, and 20 mm/s with the constant upset of 5 mm and constant oscillation frequency of 50 Hz. The formed IMC layers are bordered with solid white lines at all the joint interfaces, as shown in Fig. 9-a-i, b-i, and c-i. At the lowest forging speed of 5 mm/s, the IMC layer was observed to be thick and irregular in thickness (Fig. 9-a-i). This irregularity in thickness of the IMC layer is thought to correlate with the inhomogeneous deformation of steel that causes unevenness of the bonded interface indicated in Fig. 8b. In contrast, relatively uniform layers of IMCs were identified throughout the joint cross-section at forging speeds of 10 mm/s and 20 mm/s as shown in Fig. 9-b-i, and 9-c-i, respectively. Additionally, the average IMC layer thickness was reduced from 132.3 nm to 105.7 nm as the forging speed was increased from 5 mm/s to 10 mm/s as indicated in Fig. 9-a-ii and 9-b-ii, respectively. With a further

increase of forging speed to 20 mm/s, an extremely thin layer of IMC with an average thickness of 34.7 nm was observed at the joint interface, Fig. 9-c-ii. It is worth noting that IMC layer experienced a reduction in thickness with the increase in forging speed during LFW. This reduction in IMC layer thickness with increased forging speed can be attributed to the fact that higher forging speed resulted in lower welding heat input due to shorter weld completion time. This is a similar effect of welding speed and heat addition on IMC thickness, which was reported previously during FSW [39,40]. Namely, at a forging speed of 20 mm/s during LFW, the interfacial reaction takes place comparatively for a shorter time leading to a relatively thin IMC layer than 5 mm/s and 10 mm/s forging speeds. Yamagishi [41] obtained sound rapid dissimilar joining between SUS304 and A5083 using extremely short welding time of less than 0.1 s utilizing spot forge welding method. These results suggest that the high forging speed of 20 mm/s significantly reduced the IMC layer thickness due to the extremely short weld duration of 0.4 s and, thus resulting in the excellent tensile strength of the LFWed joint between mild steel and A7075.

Fig. 9-a-iii, b-iii, and c-iii illustrate the detailed distribution of Cu, Zn, and Mg across the interfaces of weld produced at a forging speed of 5 mm/s, 10 mm/s, and 20 mm/s, respectively. The concentration of Zn at all the interfaces was observed to increase on moving from the initiation of IMC layer towards A7075 side and revealed peak concentration over 6 at. %, at IMC/A7075 interface, in the joints produced at 5 mm/s and 10 mm/s forging speed. Whereas in the case of joint produced at 20 mm/s, peak concentration of Zn at the IMC/A7075 interface was comparatively reduced and observed to be 4.8 at. %. On the other hand, Mg was only observed in the IMCs of the joints produced at 5 mm/s and 10 mm/s forging speed. Furthermore, similar to Mg and Zn, Cu

also concentrated at the A7075/IMC interface with peak Cu concentration ranging from 6.4-8.5 at % in all the joint interfaces which is much higher than Cu concentration in A7075 base metal. It is noteworthy that the interface of the specimen fabricated at forging speed of 20 mm/s exhibits much lower concentration of Cu and Mg as compared with those of specimens fabricated at forging speed of 5 and 10 mm/s.

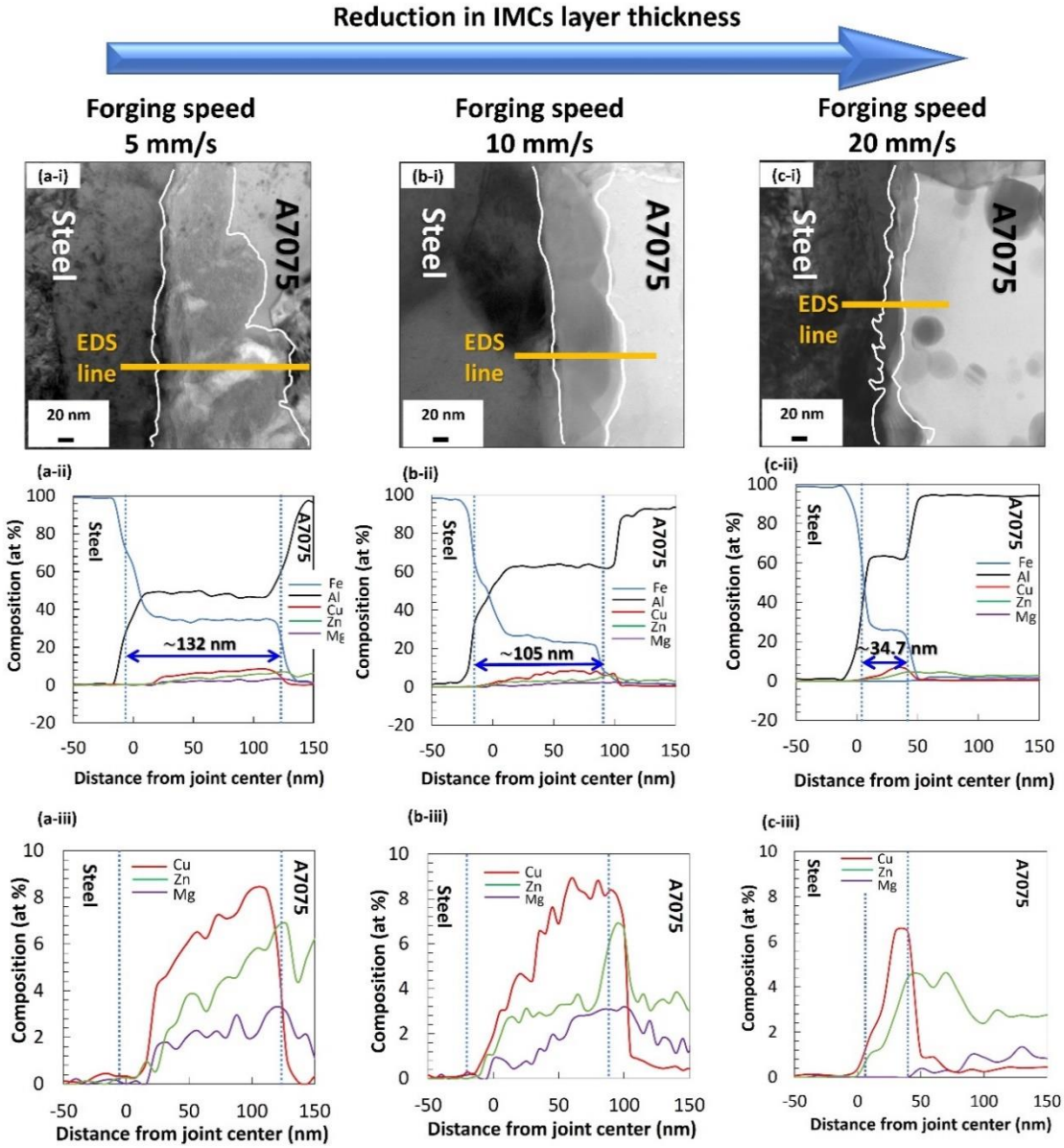

Fig. 9 TEM micrographs and EDS line scan results across the interfaces of joints fabricated at 300 MPa applied pressure and different forging speeds of 5 mm/s, 10 mm/s, and 20 mm/s.

Liu and Fang [42] conducted a study focusing on the behavior of Zn, Mg, and Cu atoms and calculated the environment-sensitive embedding energies of these elements within the matrix and at the grain boundaries of an A7XXX alloy. The Cu atoms exhibited the highest environment-sensitive embedding energies, followed by Mg, while Zn atoms had the lowest. Notably, an inverse relationship exists between an element's solubility and environment-sensitive embedding energy. Consequently, Cu displayed the lowest solubility within the aluminum matrix compared to Mg and Zn atoms [43]. On the other hand, according to Al-Cu binary phase diagram the solubility of Cu in Al increases with temperature [44]. Also, peak temperature in LFW joint during welding exist at the weld interface [45]. Therefore, it is thought that relatively elevated temperature near the interface contributed to the segregation of Cu at the joints interface. Cu was identified as having the most detrimental effect on the hot cracking sensitivity of Al alloys during welding [46,47]. Additionally, albeit to a lesser extent, presence of Mg was identified at the interface in the weld produced at 5 mm/s and 10 mm/s forging speeds. The suppression of segregation of these elements, which has a positive effect against hot cracking sensitivity of Al alloys owing to the short welding time, may also contribute to the higher strength of the weld interface. Recently, almost similar effect of high welding speed, on element segregation, weld cracking, and IMC thickness was observed during FSW [34]. The suppression of hot cracking by increasing the forging speed is in good accordance with the fact that the sound of crack was clearly heard when the forging speed was 5 and 10 mm/s, but was scarcely heard at the forging speed of 20 mm/s. A significant reduction was observed in the IMC layer thickness with increase in the forging speed from 5 mm/s to 20 mm/s. The highest IMC thickness was observed at the joint interface fabricated at lowest forging speed of 5 mm/s, followed by 10 mm/s and 20 mm/s, respectively. These

results suggest that the high forging speed of 20 mm/s significantly reduced the IMC layer thickness and concentration of Cu and Mg at the interface due to the extremely short weld duration of 0.4 s and promoted the simultaneous interfacial deformation of both alloys during LFW without the formation of the voids and cracks at the joint interface, as discussed above, thus resulting in the excellent tensile strength of the LFWed joint between steel and A7075.

3.8 TEM analysis of Al alloy and mechanism for the suppression of HAZ softening by increasing forging speed

Since the formation of precipitates plays an important role in the strength of A7075, examination of precipitates is needed in terms of their shape, size and distribution density in the interface region of Al side. Therefore, transmission electron microscope (TEM) analysis was conducted to gain further insights into hardness distribution and the occurrence of the softening region towards A7075. Fig. 10(a-c) shows the TEM images of the A7075 BM and the softening area of the weld fabricated at a forging speed of 20 mm/s and at an applied pressure of 300 MPa. Fig. 10a shows the presence of spherical precipitates in A7075 BM as indicated by the black arrows. Based on TEM observation, the precipitates were uniformly distributed, on the order of 60-90 nm in size, throughout the matrix. The magnified image of red dotted region (b) in Fig. 10a is shown in Fig. 10b, and it revealed a uniform distribution of another very fine precipitates throughout the matrix. Additionally, a narrow precipitate-free zone (PFZ), approximately 30 nm wide, was identified along the grain boundaries. Furthermore, Fig. 10c illustrates the TEM image of the softened region of the obtained weld, located 2 mm away from the weld center. In this region, TEM investigation revealed the complete dissolution of very fine precipitates due to the elevated temperatures during LFW. Moreover, the distribution of

spherical precipitates, similar to those in the BM, was also observed in the matrix along with rod-shaped precipitates, as indicated by red arrows in Fig. 10c. The existence of rod-shaped precipitates indicates that the precipitates within the base metal had undergone partial dissolution due to high temperature during LFW, followed by reprecipitation during cooling, a phenomenon consistent with prior research findings [48]. It was thought that the cooling rate was such that the coarser precipitates could nucleate and grow, but the finer ones could not nucleate [49]. In other words, in the range of joining conditions used in this study, the softening in HAZ of A7075 is suppressed by decrease of heat input. This is consistent with the noticeable suppression of HAZ softening of the joint at a forging speed of 20 mm/s, where the required welding time is short and the heat input is small, as shown in Fig. 3.

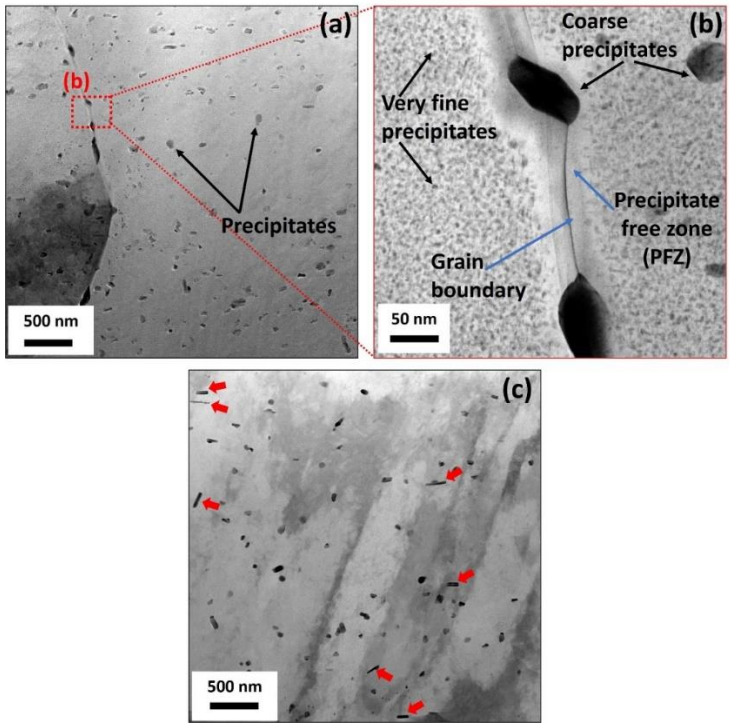

Fig. 10 TEM micrographs of (a) A7075 BM, (b) Magnified image of red dotted square in (a), (c) softening zone of weld fabricated at an applied pressure and forging speed of 300 MPa and 20 mm/s, respectively.

4. Conclusion

Sound dissimilar LFW joint between A7075 and mild steel was successfully obtained based on the optimization of applied pressure and forging speed. The influence of the forging speeds on mechanical properties and joint interfacial macrographs was investigated. The obtained results are concluded as follows.

(1) An applied pressure of 100 MPa and 5 mm/s forging speed was found effective to facilitate interfacial deformation towards A7075 only, whereas no interfacial deformation towards the faying surface of steel was identified during welding due to the huge difference in the strength between mild steel and A7075.

(2) When the pressure was applied 300 MPa, corresponding to common point of intersection of the strength of both alloys, faying surface of steel experienced gradient deformation at lower forging speed. The obtained welds exhibited poor joint strength due to the occurrence of several weld defects and un-bonded regions at the joint interface.

(3) Higher forging speed of 20 mm/s was found effective to completely suppress the joint defects by promoting simultaneous interfacial deformation of both alloys during welding, which led to a sound joint without any interfacial un-bonded areas.

(4) IMC layer was observed to be reduced with the increase in forging speed. At an applied forging speed of 20 mm/s, extremely thin layer of IMC, with an average thickness of 34.7 nm, was identified at the joint interface. Furthermore, the enrichment of Cu and Mg in the interface was also suppressed. Higher forging speed reduced the required welding time and duration of heat, which eventually reduced the heat input during welding. Therefore, the simultaneous interface plastic deformation of both alloys without the formation of voids and cracks became

possible.

(5) Weld fabricated at an applied pressure of 300 MPa and 20 mm/s forging speed revealed excellent joint strength exhibiting 100 % joint efficiency with respect to steel. The fracture was located in the base metal region of steel.

Conflict of interest

The authors declare no conflict of interest.

Acknowledgement

The authors appreciate the Innovative Structural Materials Association (ISMA) for providing the center-drive double-sided LFW equipment. This work was supported by the JST-Mirai Program [grant number JPMJMI19E5] and a grant-in-aid for scientific research from the Japan Society for the Promotion of Science [grant number 19H00826].

References

[1] Liu T, Gao S, Ye W, Shi L, Kumar S, Qiao J. Achievement of high-quality joints and regulation of intermetallic compounds in ultrasonic vibration enhanced friction stir lap welding of aluminum/steel. J Mater Res Technol 2023;25:5096–109. https://doi.org/10.1016/j.jmrt.2023.06.251.

[2] Hsieh MJ, Lee RT, Chiou YC. Friction stir spot fusion welding of low-carbon steel to aluminum alloy. J Mater Process Technol 2017;240:118–25. https://doi.org/10.1016/j.jmatprotec.2016.08.034.

[3] Kar A, Vicharapu B, Morisada Y, Fujii H. Elucidation of interfacial microstructure and properties in friction stir lap welding of aluminium alloy and mild steel. Mater Charact 2020;168:110572. https://doi.org/10.1016/j.matchar.2020.110572.

[4] Zhang D, Qin G, Geng P, Ma H. Study of plastic flow on intermetallic compounds formation in friction welding of aluminum alloy to stainless steel. J Manuf Process 2021;64:20–9. https://doi.org/10.1016/j.jmapro.2021.01.019.

[5] Dong H, Yang J, Li Y, Xia Y, Hao X, Li P, et al. Evolution of interface and tensile properties in 5052 aluminum alloy/304 stainless steel rotary friction welded joint after post-weld heat treatment. J Manuf Process 2020;51:142–50. https://doi.org/10.1016/j.jmapro.2020.01.038.

[6] Mahto RP, Kumar R, Pal SK, Panda SK. A comprehensive study on force, temperature, mechanical properties and micro-structural characterizations in friction stir lap welding of dissimilar materials (AA6061-T6 & AISI304). J Manuf Process 2018;31:624–39. https://doi.org/10.1016/j.jmapro.2017.12.017.

[7] Yao Y, Jing L, Wang S, Li G, Cui J, Tang X, et al. Mechanical properties and joining mechanisms of Al-Fe magnetic pulse welding by spot form for automotive application. J Manuf Process 2022;76:504–17. https://doi.org/10.1016/j.jmapro.2022.02.017.

[8] Zhang C, Cui G, Chen B, Liu X, Shi Y, Wang Y. Effect of Ag interlayer on friction torque, mechanical properties and microstructure of large diameter aluminum/steel joints by continuous drive friction welding. J Manuf Process 2022;78:341–51. https://doi.org/10.1016/j.jmapro.2022.04.006.

[9] Zhao Y, Wang Q, Chen H, Yan K. Microstructure and mechanical properties of spray formed 7055 aluminum alloy by underwater friction stir welding. Mater Des (1980-2015) 2014;56:725–30. https://doi.org/10.1016/j.matdes.2013.11.071.

[10] Xu W, Li Z, Sun X. Effect of welding speed on mechanical properties and the strain-hardening behavior of friction stir welded 7075 aluminum alloy joints. J Mater Eng Perform 2017;26:1938–46. https://doi.org/10.1007/s11665-017-2618-6.

[11] Sokoluk M, Cao C, Pan S, Li X. Nanoparticle-enabled phase control for arc welding of unweldable aluminum alloy 7075. Nat Commun 2019;10:98. https://doi.org/10.1038/s41467-018-07989-y.

[12] Yang T, Dai W, Zhuang Y, Liu J, Zhou Z, Hu J. Investigation on the control of interfacial layer uniformity in laser-metal inert-gas hybrid welded-brazed Al/steel butt joint. J Manuf Process 2020;58:1241–50. https://doi.org/10.1016/j.jmapro.2020.09.045.

[13] Hu S, Haselhuhn AS, Ma Y, Li Y, Carlson BE, Lin Z. Sensitivity of dissimilar aluminum to steel resistance spot welds to weld gun deflection. J Manuf Process 2021;68:534–45. https://doi.org/10.1016/j.jmapro.2021.05.059.

[14] Hu S, Haselhuhn AS, Ma Y, Li Z, Qi L, Li Y, et al. Effect of external magnetic field on resistance spot welding of aluminium to steel. Sci Technol Weld Join 2022;27:84–91. https://doi.org/10.1080/13621718.2021.2013707.

[15] Herbst S, Aengeneyndt H, Maier HJ, Nürnberger F. Microstructure and mechanical properties of friction welded steel-aluminum hybrid components after T6 heat treatment. Mater Sci Eng A 2017;696:33–41. https://doi.org/10.1016/j.msea.2017.04.052.

[16] Tanaka T, Morishige T, Hirata T. Comprehensive analysis of joint strength for dissimilar friction stir welds of mild steel to aluminum alloys. Scr Mater 2009;61:756–9. https://doi.org/10.1016/j.scriptamat.2009.06.022.

[17] Kawai G, Ogawa K, Ochi H, Tokisue H. Friction weldability of aluminium alloys to carbon steel. Weld Int 2000;14:101–7. https://doi.org/10.1080/09507110009549147.

[18] Kimura M, Kusaka M, Kaizu K, Hayashida K. Simultaneous friction welding and characterization of joints between 7075-t6 al alloy and low-carbon steel using pure al as an insert metal. J Mater Eng Perform 2019;28:7726–36. https://doi.org/10.1007/s11665-019-04507-z.

[19] Kimura M, Yukawa T, Kusaka M, Kaizu K, Fuji A. Possibility of direct friction welding between type 7075 aluminum alloy and low carbon steel. Proceedings of the 1st International Joint Symposium on Joining and Welding, Elsevier; 2013; 267–73. https://doi.org/10.1533/978-1-78242-164-1.267.

[20] W. Richter. Creation of an adhesive bond between plaques of tool steel and their supports in the manner of welding or soldering. Germany Patent DE477084, 1929. (in German)

[21] Maurya R, Kauzlarich J. Bonding apparatus - friction welding by reciprocal motion. US Patent 3420428-A, UK Patent GB1161800 A, 1969.

[22] Dalgaard E, Wanjara P, Gholipour J, Cao X, Jonas JJ. Linear friction welding of a near-β titanium alloy. Acta Mater 2012;60:770–80. https://doi.org/10.1016/j.actamat.2011.04.037.

[23] Wanjara P, Jahazi M. Linear friction welding of Ti-6Al-4V: Processing, microstructure, and mechanical-property inter-relationships. Metall Mater Trans A 2005;36:2149–64. https://doi.org/10.1007/s11661-005-0335-5.

[24] Mary C, Jahazi M. Linear friction welding of IN-718 process optimization and microstructure evolution. Adv Mat Res 2006;15–17:357–62. https://doi.org/10.4028/www.scientific.net/AMR.15-17.357.

[25] Fujii H. Low-temperature linear friction welding of metal and alloys with 100% joint efficiency. Keikinzoku Yosetsu/Journal of Light Metal Welding 2020;58:8–13. https://doi.org/10.11283/jlwa.58.8s.

[26] Guo Z, Ma T, Yang X, Li J, Li W, Vairis A. Multi-scale analyses of phase transformation mechanisms and hardness in linear friction welded Ti17(α + β)/Ti17(β) dissimilar titanium alloy joint. Chin J Aeronaut 2023 (Online). https://doi.org/10.1016/j.cja.2023.08.018.

[27] Guo Z, Ma T, Yang X, Tao J, Li J, Li W, et al. In-situ investigation on dislocation

slip concentrated fracture mechanism of linear friction welded dissimilar Ti17(α+β)/Ti17(β) titanium alloy joint. Mater Sci Eng A 2023;872:144991. https://doi.org/10.1016/j.msea.2023.144991.

[28] Buffa G, Cammalleri M, Campanella D, La Commare U, Fratini L. Linear friction welding of dissimilar AA6082 and AA2011 aluminum alloys: microstructural characterization and design guidelines. Int J Mater Form 2017;10:307–15. https://doi.org/10.1007/s12289-015-1279-y.

[29] Kimura M, Nakashima K, Kusaka M, Kaizu K, Nakatani Y, Takahashi M. Joining phenomena and tensile strength of joint between Ni-based superalloy and heat-resistant steel by friction welding. Int J Adv Manuf Technol 2019;103:1297–308. https://doi.org/10.1007/s00170-019-03611-7.

[30] Lim Y, Morisada Y, Liu H, Fujii H. A sound dissimilar AA5052/S45C joint formed by uniform and simultaneous deformation of both materials using pressure-controlled joule heat forge welding. ISIJ Int 2022;62:1715–24. https://doi.org/10.2355/isijinternational.ISIJINT-2022-034.

[31] Bhamji I, Preuss M, Threadgill PL, Addison AC. Solid state joining of metals by linear friction welding: a literature review. Mater Sci Technol 2011;27:2–12. https://doi.org/10.1179/026708310X520510.

[32] Senkova SV, Senkov ON, Miracle DB. Cryogenic and elevated temperature strengths of an Al−Zn−Mg−Cu alloy modified with Sc and Zr. Metall Mater Trans A 2006;37:3569–75. https://doi.org/10.1007/s11661-006-1051-5.

[33] Anderson, T. How to avoid cracking in aluminum alloys. Weld J 2005;84:25–7.

[34] Saleh M, Morisada Y, Ushioda K, Fujii H. Sound dissimilar friction stir welded joint of mild steel and A7075 aluminum alloy by increasing welding speed. Mater Today Commun (under review). https://dx.doi.org/10.2139/ssrn.4543155.

[35] Cheng CM, Chou CP, Lee IK, Lin HY. Hot cracking of welds on heat treatable aluminium alloys. Sci Technol Weld Join 2005;10:344–52. https://doi.org/10.1179/174329305X40688.

[36] Matsuda T, Adachi H, Sano T, Yoshida R, Hori H, Ono S, et al. High-frequency linear friction welding of aluminum alloys to stainless steel. J Mater Process

Technol 2019;269:45–51. https://doi.org/10.1016/j.jmatprotec.2019.01.023.

[37] Ochi H, Ogawa K, Yamamoto Y, Kawai G, Tsujino R, Suga Y. Effect of intermetallic compounds on friction weldability of aluminum alloys to S25C carbon steel. J Soc Mater Sci 2004;53:532–8. https://doi.org/10.2472/jsms.53.532.

[38] Nakashima R, Fuji A, Tohkuni H, Kimura M. friction welding of A7075/low carbon steel joint-Study with insert material. Preprints of the National Meeting of JWS, 2010;87:15-16, doi: 10.14920/jwstaikai.2010f.0.7.0. (in Japanese)

[39] Chen YC, Komazaki T, Kim YG, Tsumura T, Nakata K. Interface microstructure study of friction stir lap joint of AC4C cast aluminum alloy and zinc-coated steel. Mater Chem Phys 2008;111:375–80. https://doi.org/10.1016/j.matchemphys.2008.04.038.

[40] Kimapong K, Watanabe T. Lap joint of A5083 aluminum alloy and SS400 steel by friction stir welding. Mater Trans 2005;46:835–41. https://doi.org/10.2320/matertrans.46.835.

[41] Yamagishi H. Spot forge-welding for rapid dissimilar joining of Fe to Al to produce an intermetallic compound-free interface. Mater Trans 2021;62:MT-M2021080. https://doi.org/10.2320/matertrans.MT-M2021080.

[42] Guili L, Fang G. Grain-boundary segregation and corrosion mechanism of Al-Zn-Mg-Cu ultra high strength aluminum alloys. Rare Metal Mat Eng 2009;38:1598–601.

[43] Yang X, Li Y, Luo X, Zhou H, Cai Q, Li M, et al. Microstructural evaluation and mechanical properties of 7075 aluminum alloy prepared by controlled diffusion solidification. China Foundry 2019;16:238–47. https://doi.org/10.1007/s41230-019-9059-9.

[44] Zobac O, Kroupa A, Zemanova A, Richter KW. Experimental description of the Al-Cu binary phase diagram. Metall Mater Trans A 2019;50:3805–15. https://doi.org/10.1007/s11661-019-05286-x.

[45] Jedrasiak P, Shercliff HR. Modelling of heat generation in linear friction welding using a small strain finite element method. Mater Des 2019;177:107833. https://doi.org/10.1016/j.matdes.2019.107833.

[46] Matsuda F, Nakata K, Shimokusu Y, Tsukamoto K, Arai K. Effect of additional element on weld solidification crack susceptibility of Al-Zn-Mg alloy (Report I). Materials, Metallurgy &, Citation Transactions of JWRI 1983;12:81–87. https://doi.org/10.18910/9991.

[47] Bozorgi S, Haberl K, Kneissl C, Pabel T, Schumacher P. Effect of alloying elements (Magnesium and Copper) on hot cracking susceptibility of $AlSi_7MgCu$ alloys. Shape Casting, Wiley 2011;113–20. https://doi.org/10.1002/9781118062050.ch14.

[48] Choi J-W, Li W, Ushioda K, Fujii H. Flat hardness distribution in AA6061 joints by linear friction welding. Sci Rep 2021;11:11756. https://doi.org/10.1038/s41598-021-91249-5.

[49] Rhodes CG, Mahoney MW, Bingel WH, Spurling RA, Bampton CC. Effects of friction stir welding on microstructure of 7075 aluminum. Scr Mater 1997;36:69–75. https://doi.org/10.1016/S1359-6462(96)00344-2.